Structural determination of a highly stable metal-organic framework with possible application to interim radioactive waste scavenging: Hf-UiO-66

S. Jakobsen, D. Gianolio, D. S. Wragg, M. H. Nilsen, H. Emerich, S. Bordiga, C. Lamberti, U. Olsbye, M. Tilset, K. P. Lillerud
"Structural determination of a highly stable metal-organic framework with possible application to interim radioactive waste scavenging: Hf-UiO-66",
Phys. Rev. B. **86** (2012) Art. n. 125429

DOI: 10.1103/PhysRevB.86.125429

Structural determination of a highly stable metal-organic framework with potentials in interim radioactive waste scavenging: Hf-UiO-66

Søren Jakobsen,[1] Diego Gianolio,[2] David Wragg,[1] Merete Hellner Nilsen,[1] Hermann Emerich,[3] Silvia Bordiga,[4] Carlo Lamberti,[4,*] Unni Olsbye,[1] Mats Tilset[1] and Karl Petter Lillerud[1]

[1] *SMN/INGAP/Department of Chemistry. University of Oslo Sem Selands vei 26, 0315 Oslo, Norway*
[2] *Diamond Light Source Ltd, Harwell Science and Innovation Campus, OX11 0DE, Didcot (UK)*
[3] *Swiss Norwegian Beamlines (SNBL) at the European Synchrotron (ESRF) in Grenoble, France.*
[4] *Department of Chemistry NIS Centre of Excellence, and INSTM reference center, University of Turin, Via P. Giuria 7, I-10125 Torino, 4 Italy.*

Abstract

High resolution synchrotron radiation x-ray powder diffraction (HR-XRPD) combined with Hf L3-edge extended x-ray absorption fine structure (EXAFS) allowed to determine the structure of Hf-UiO-66 metal-organic framework (MOF) showing that it is iso-reticular to Zr-UiO-66 MOF [J. Am. Chem. Soc. 130, 13850 (2008)]. Thermal gravimetric measurements (coupled with mass spectroscopy) and temperature dependent synchrotron radiation XRPD proved the high thermal stability of the new MOF. The Langmuir surface area (849 m^2/g) combined with the high stability of the UiO-66 framework and with the high neutron absorption cross section of Hf suggest that among all microporous crystalline materials the new Hf-UiO-66 MOF possesses the physical and chemical requirements for the interim storage of radioactive waste in a much safer way than is currently available. The first results proving the synthesis of a MOF material with UiO-66 topology realized by B-containing linker are also reported, allowing a further improvement of the neutron shielding power of these class of materials.

Principal PACS : 81.07.Pr Organic-inorganic hybrid nanostructures
Additional PACS: 61.05.cp X-ray diffraction;
61.05.cj X-ray absorption spectroscopy: EXAFS,
28.41.Kw Radioactive wastes, waste disposal

I. INTRODUCTION

Metal-Organic Frameworks (MOFs) have received much attention the past decade and a huge number of new materials with a wide range of different compositions and properties have been reported.[1-4] The most sought after MOF materials are those with internal open-pore systems exhibiting some of the main properties of the traditional porous materials, zeotype and mesoporous materials. The highest specific surface area materials are now found within MOFs[5] that, being constructed directly from simple organic molecules and metal salts, allow to tailor their chemical composition and physico-chemical properties to a large extent towards any given application. Although the industrial application of MOFs is still limited to few cases,[6] these materials being three-dimensional polymers of alternating metal/metal cluster and organic units have already shown potentialities in: (i) gas storage;[7-15] (ii) gas separation and purification;[16,17] liquid phase separation;[18] (iii) drug delivery;[19,20] (iv) catalysis[21,22] (v) molecular sensors;[23] and (vi) solid state ion conduction.[24] Moreover, MOFs can represent a new class of optical,[25-27] magnetic[28] and semi-conducting[29] materials. Finally, some MOFs exhibit interesting mechanical[30,31] and diffusive[32] properties. Here we present the synthesis and the structural characterization of a highly stable and absorbing MOF with potentials in interim radioactive waste scavenging: Hf-UiO-66.

The safe short and long term storage of nuclear wastes of civil (both working and spent nuclear plants are involved) and military origin still represents a challenging multidisciplinary scientific

problem, that has relevant social, economical and political issues,[33-38] needing scientific competencies in physics, chemistry, materials science, engineering and geology to be faced. During the past half-century, the nuclear fuel cycle has generated more than 1500 metric tons of plutonium and substantial quantities of the "minor" actinides, such as Np, Am, and Cm.[39] The successful disposition of these actinides has an important impact on the strategy for developing advanced nuclear fuel cycles and the geologic disposal of high-level radioactive waste.[34,36,37,40-42]

Different classes of materials have been used for the interim immobilization of actinides,[43] among them, e. g. ceramics,[44-48] perovskite,[49,50] natural silicates,[51] and glasses.[48,52] Among porous materials, silica aerogels[53] and zeolites[54,55] (i.e. crystalline porous aluminosilicates) have already proven to be useful in radioactive waste management, by their ability to adsorb guest species into an internal pore system. However their composition of light, weakly radiation-absorbing elements limits the usefulness of these materials to the encapsulation stage only, without any ability to significantly adsorb the radiation emitted by the hosted radioactive species. MOFs, on the other hand, can be constructed from strongly radiation-absorbing metals (such as Hf), while the organic parts may bear strongly neutron absorbing nuclei (such as B). Additional requirements from such a MOF are large internal volume to store waste material combined with very high thermal and chemical robustness to keep structural integrity and handling safe. Only very few MOF materials exhibit both large internal volumes and thermal and chemical stabilities and, up to now, none of them incorporate any kind of substantial radiation-absorbing metals or linkers. An important member of this restricted family is the zirconium-based MOF UiO-66 reported by us in 2008.[56] The potentialities of this new material have been immediately realized by the scientific community and many UiO-66 derived structures and modifications have already been published so far by several groups worldwide.[57-70]

In this work we report on the synthesis, thermo gravimetric analysis (TGA), synchrotron radiation x-ray powder diffraction (XRPD), and extended x-ray absorption fine structure (EXAFS) analysis of the crystal structure of the Hf-equivalent UiO-66 (hereafter Hf-UiO-66), where Hf atoms substitutes isomorphically Zr ones in the inorganic cornerstones. The high electron number of Hf (Z = 72) and its large neutron absorption cross section (σ_{abs} = 0.185(3); barn: 1 barn = 10^{-28} m^2)[71] makes this new member of the UiO-66 family interesting for potential interim storage of radioactive waste. Moreover, the use of linkers incorporating boron atoms (σ_{abs} = 767(8) barn) will further improve the potentialities of this class of microporous materials for this goal.

After the first submission of this manuscript, Lin group succeeded in the synthesis of a bimetallic Zr-Hf-UiO-66 (Zr 37 wt% and Hf 57 wt%).[72] This interesting study shows the potentiality of this new material as contrast agent for computed tomography imaging inside living tissues. The increasing contrast power of Zr-Hf-UiO-66 is based on the presence of very high-Z (Hf) and relatively high-Z (Zr) atoms. The synthesis of a 100 wt% Hf material presented in this work results in a material that will be more efficient also for the interesting computed tomography imaging application presented in the recent Lin work.[72]

II. EXPERIMENTAL AND METHODS

A. Materials synthesis

The synthesis of Zr-UiO-66, here used for comparison, has been described elsewhere.[56] As for Hf-UiO-66, 150 mg $HfCl_4$ (0.47 mmol), 87 mg terephthalic acid (0.52 mmol) were mixed in 5 ml dimethylformamide (DMF) containing 0.1 M H_2O. The sealed glass vessel was heated to 100 °C for 24 h, cooled to RT and filtered, resulting in the desired Hf-UiO-66, MOF material.

Boron-functionalized UiO-66 was synthesized as follows: 11.7 mg of $ZrCl_4$ and 11.6 mg *p*-carborane-dicarboxylic acid[73] was mixed in 4 ml DMF. The synthesis mixture was transferred to a Teflon liner, and left to crystallize in a autoclave at 120°C for 24 h, before cooled to room temperature and filtered.

B. Laboratory techniques

Standard XRPD measurement was performed on a Bruker D5000 instrument with monochromatic CuKα1 radiation (λ = 1.540 Å) operated in Bragg-Bretano geometry and a variable slit. The instrument was equipped with a sample changer for XRPD plates giving non-transmission XRPD diffractograms. All data was collected at ambient temperature in air.

Specific surface areas were determined from nitrogen adsorption/desorption isotherms and were performed on a BEL SORP MINI system (BEL Japan, Inc.) at −196 °C. The sample was activated before measurement under vacuum at 1 h at 90 °C and then 2 h at 300 °C. The total surface area was determined by the BET and Langmuir methods, based on p/p_0 data in the range of 0.0-1.0.

Thermogravimetric analysis (TGA) was carried out in either pure flowing nitrogen or a 20 % mixture of oxygen in nitrogen using a Rheometric Scientific STA 1500 instrument with an adapted gas supply system. The TGA analyses were performed with parallel in-line mass spectrometric (MS) analysis collecting sample app. 3 mm above the sample inside the TGA equipment. The MS data were recorded with a Pfeiffer OmniStar GSD 300 O quadrupole equipped with an electron multiplier detector. The approximate sample weight was 10 mg in all experiments and the heating rate in TGA experiments was 5 °C/min.

C. Synchrotron radiation techniques and corresponding data analysis

Both x-ray diffraction and absorption experiments were performed at the BM01B of the Swiss-Norwegian beamlines (SNBL) of the European Synchrotron Radiation facility (ESRF). This beamline has the peculiarity of having two different monochromators that can be inserted or removed from the x-ray optic path in a plug and ply way, so allowing to switch on the same sample from high resolution x-ray powder diffraction (HR-XRPD) to XAFS data collection, or vice versa, in less than one minute time. In order to follow *in situ* (with both HR-XRPD and XAFS techniques) the activation and the thermal stability of Hf-UiO-66, a sample was hosted inside an open capillary (1 mm in diameter) acting as reaction tube where the sample temperature can be increased with a programmed ramp using a heat-gun while fluxing the sample by inert gas to evacuate removed solvent molecules, using set-ups similar to those reported elsewhere.[74,75]

A Rietveld refinement of the structure of Hf-UiO-66 was carried out HR-XRPD data collected at BM01B. Data were collected at room temperature over a 2θ range of 0.7 to 50 degrees with a wavelength of 0.50114(4) Å delivered by a Si(111) channel-cut monochromator ($d_{spacing}$ = 0.59 Å). HR-XRPD patterns were collected in a continuous scanning mode, with the electronic scalers and the 2θ encoder read around 6 times per second. The high-angle regions being scanned more than once to improve the statistical quality of the pattern. The detector bank consists of six scintillator counters, each behind a separate Ge(111) analyzer crystal, with the six crystals mounted on a single rotation stage. The separation between each channel is close to 2°. Consequently, nine diffraction patterns, offset one from the other by around 2°, are measured simultaneously. The counts from the six channels collected at the various positions during the scan are rebinned, taking account of the exact separation between the channels, the different detector efficiencies, and the decrease in the beam current during the scan, to produce the equivalent normalized step scan, which is more suitable for analysis by standard Rietveld programs. Rejection of the harmonics, (mainly λ/3), that are transmitted by the channel cut monochromator and the analyzer crystals is achieved by setting the electronic windows on the detector electronics. Rietveld refinement[76] was carried out using the program TOPAS academic.[77] The instrumental peak shape was modeled by fitting a set of convolutions to a pattern for NIST standard lanthanum hexaboride SRM660a, which was also used for the wavelength calibration.

EXAFS measurements were performed at the Hf L_3-edge (9561 eV). The white beam was monochromatized using a Si(111) double crystal; harmonic rejection was performed by detuning the crystals to 60% of the maximum flux. EXAFS spectra were collected in transmission mode. Ionization chambers measuring I_0 and I_1 were filled with 1 bar of 100% N_2 and 85% N_2 and 15% Ar, resulting in an absorption efficiency of 15 and 50% of the x-ray beam, respectively. The beam

was vertically slit down to reach a dimension on the sample of 0.3 mm. For the XAFS spectrum collected with the sample at room temperature (as-synthesized material) the pre-edge region was acquired with an energy step of 5 eV and an integration time of 1 s/point, the XANES part with a more fine energy step of 0.3 eV and same integration time. EXAFS part of the spectra were collected up to 17 $Å^{-1}$ with a variable sampling step in energy, resulting in $\Delta k = 0.05$ $Å^{-1}$, and an integration time that linearly increases with k from 2 to 5 s/point to account for the low signal-to-noise ratio at high k values. During the heating ramp, the EXAFS spectra were acquired in quick-EXAFS mode with an average sampling step of about 1 eV collected in about 0.5 s. Once the heat gun reached the plateau of 300 °C, three successive spectra were collected under isothermal condition. The averaged EXAFS spectrum has been used to refine the local structure of the activated material. The difference in the signal to noise of the two data sets is due to the higher collection temperature of the second spectrum (resulting in higher Debye-Waller factors) and to the different acquisition procedures.

EXAFS data analysis has been performed using the Artemis software.[78] Phase and amplitudes have been calculated by FEFF8 code.[79] using as input the structures optimized by XRPD and following the same refinement strategy already optimized for the Zr-homologe of UiO-66.[80] For the as prepared sample, the k^2-weighted $\chi(k)$ functions were Fourier transformed in the $\Delta k = 2.0\text{-}16.0$ $Å^{-1}$ interval, then the fit was performed in R-space in the $\Delta R = 1.0\text{-}5.5$ Å range. The number of independent points resulting from the selected ranges is $2 \cdot \Delta k \cdot \Delta R/\pi > 40$. The lower signal to noise ratio of the spectrum relative to the sample measured at 300 °C forced us to work on restricted intervals: $\Delta k = 2.0\text{-}15.0$ $Å^{-1}$ and $\Delta R = 1.0\text{-}3.9$ Å, resulting in $2 \cdot \Delta k \cdot \Delta R/\pi > 25$.

In the EXAFS data analysis of the Hf-UiO-66 sample measured at room temperature, we have considered altogether 10 paths. A single parameter, common for all the paths, was used both for amplitude factor (S_0^2) and energy shift (ΔE_0). Two Single Scattering (SS) paths involving oxygen (μ3O and O) contributes to the first shell signal at about 1.8 Å. In the 2–3 Å region there is an superposition of different paths: a SS Hf-C path and many triangular Multiple Scattering (MS) involving both oxygen and carbon atoms of the organic linkers. Lastly, the big signal around 3.4 Å is assignable to a strong Hf-Hf_1 SS path with degeneration 4 as the number of Hf atoms neighbors of the absorber in the octahedral $Hf_6O_4(OH)_4$ cluster. It was also possible to isolate the signal due to the SS path involving the single Hf_2 atom in the opposite position of the octahedron.

For each SS path two parameter were optimized: the distance and the Debye-Waller Factor. For the two different oxygen atoms (μ3O and O) in the first shell a common Debye-Waller factor σ^2_O was used. For the MS we used a linear combination of the parameters related to all the atoms involved. The R_{Hf2} diagonal distance was parameterized by following geometrical rules ($R_{Hf1} \cdot \sqrt{2}$).[80]

III. Results and discussion

A. Assessment of crystalline phase, porosity and thermal stability of Hf-UiO-66: comparison with Zr-UiO-66

UiO-66 consists of hexanuclear, octahedral zirconium oxo-clusters connected through terephthalic dicarboxylate linkers to form a three-dimensional, highly porous rigid and massive framework,[56,80] see inset in Fig. 1a. This is reflected in its thermal stability, as it stays intact even at temperatures above the breakdown temperature of pure terephthalic acid. Crystallinity is maintained even above 400 °C in air and has been shown to tolerate a wide range of different solvents including water acids and bases.[56,70,80] We present here a thorough investigation of a new hafnium-containing MOF, Hf-UiO-66, with the same topology and stability as the Zr-UiO-66 MOF but with the added potential for uses within radiation hosting, scavenging and protecting (vide infra Section III.C). The Hf-UiO-66 MOF was prepared by a slightly modified method compared to that originally published for Zr-UiO-66 (see Section II.A) and was identified by laboratory XRPD. The XRPD of Hf-UiO-66 index to exactly the same cubic cell as the UiO-66 zirconium analog with only slight differences in relative intensities, but not more than expected from the replacement of

zirconium with the heavier hafnium (Fig. 1a). The two main peaks in the diffractogram are the (111) and (002) reflections, 2θ = 7.42 and 2θ = 8.57 degrees, respectively. At 2θ lower than the (111) reflection, two broad peaks of lower intensity are observed for the Hf-UiO-66 sample. These represents forbidden reflections for the topological space group (*Fm-3m* , 225), but these broad peaks index in the right cubic cell if the symmetry is reduced to primitive. These peaks disappear upon activation (pattern not reported), and are clearly a solvent effect.

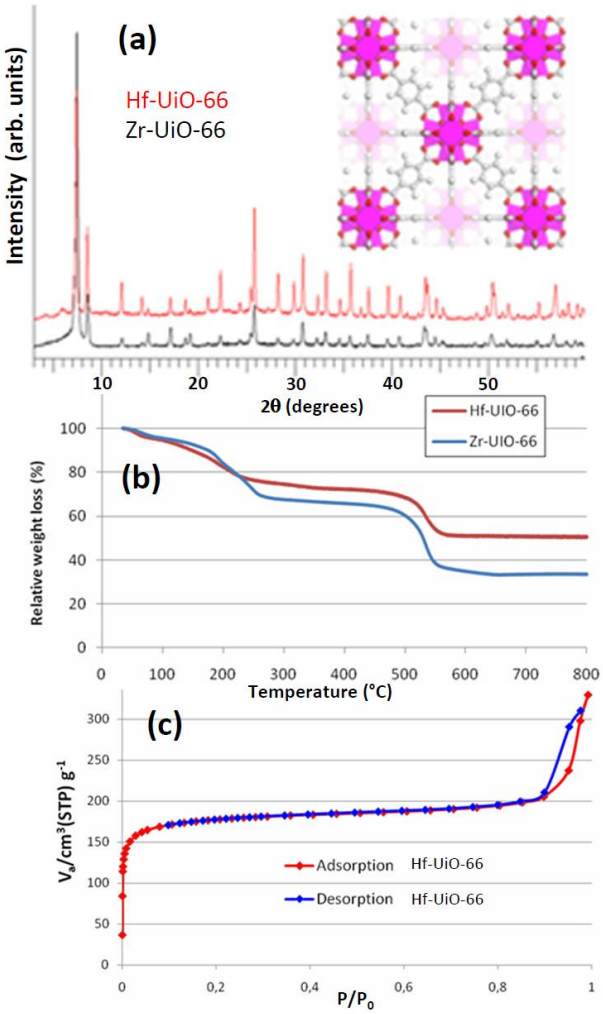

Fig. 1. Part (a): XRPD pattern (λ=1.540 Å) of hafnium containing UiO-66, Hf-UiO-66 (red) and zirconium containing UiO-66 (black) in their solvated forms (i.e. with DMF solvent in the pores). The inset reports the MOF structure viewed one of the 3 equivalent *a*, *b* or *c* directions. Part (b) Weight loss of Hf-UiO-66 relative to the start mass (red curve). The weight loss of Zr-UiO-66 has been added as a reference (blue curve). Since hafnium is 41% heavier than zirconium, the Zr-UiO-66 shows both higher initial and breakdown losses. Part (c): N_2 adsorption/desorption isotherm for Hf-UiO-66. at −196 °C.

The TGA-curve comparing as-synthesized Hf-UiO-66 and Zr-UiO-66 are shown in Fig. 1b, red and blue curves, respectively. Mass spectroscopy, coupled with the TGA experiment shows that the weight loss in the 150–200 °C temperature interval is due to the release of the DMF solvent (m/z = 73, 57, 44 and 43). After the stability plateau, the weight loss in the 500–750 °C temperature interval is mainly due to CO_2 (m/z = 44) and benzene (m/z = 78) demonstrating the framework breakdown. These data prove that the high thermal stability of the framework is not compromised by the substitution of Zr by Hf, as the structure collapse is due to the break of the linker-cornerstone bonds and not to the degradation of the cornerstone itself. Quantitative numbers reported in Table 1 testifies that, in first approximation, the mass left at the end of the TGA run is that expected for the HfO_2 or ZrO_2 combustion products. The discrepancy between the experimental residual weight at

the end of the TGA run and the stoichiometric value has been explained for the Zr-UiO-66 as due to framework defectivity: lack of some linkers connecting adjacent inorganic corner stones.[80]

Table 1. Comparison of thermogravimetric analysis of Hf-UiO-66 and Zr-UiO-66 reported in Fig. 1b.

	Hf-UiO-66		Zr-UiO-66	
Temperature interval	Measured	Stoichiometric [b]	Measured	Stoichiometric [b]
25–400 °C (Solvent removal)	28 %	—	34 %	—
400–700 °C (Structural breakdown)[a]	30 %	41 %	49 %	55 %

[a] Relative % from the activated mass.

[b] MO_2 (M = Hf or Zr) is assumed to be the only breakdown product.

To investigate the potential of Hf-UiO-66 for molecular storage in general (and for radioactive molecules in particular), its internal surface was analyzed by nitrogen adsorption. Evaluation of the resulting isotherm gave, after correcting for the higher atomic mass of Hf relative to Zr, specific molar surface areas comparable to Zr-UiO-66 (Table 2 and Fig. 1c), which confirms the full availability of large internal volumes.

Table 2. Surface areas of Hf-UIO-66 compared to Zr-UIO-66.

		BET (m^2/g)		Langmuir (m^2/g)	
Metal	Unit cell	Measured	Pr. mole unit cel	Measured	Pr. mole unit cel
Hf	$Hf_{24}O_{120}C_{192}H_{96}$	655	$9.40\ 10^{05}$	849	$1.22\ 10^{06}$
Zr	$Zr_{24}O_{120}C_{192}H_{96}$	1024	$11.1\ 10^{05}$	1297	$1.41\ 10^{06}$

B. Structural refinement

1. HR-XRPD refinement of the solvated Hf-UiO-66 material

To further compare Hf-UiO-66 to Zr-UiO-66 high quality XRPD data were needed. Unfortunately employing standard laboratory sources (Fig. 1a) the medium and high 2θ reflections are severely affected by sample adsorption (due to Hf content), making Rietveld refinement delicate. To overcome this radiation absorption problem low λ and high flux synchrotron radiation high resolution (HR)-XRPD data was collected and refined (Fig. 2).

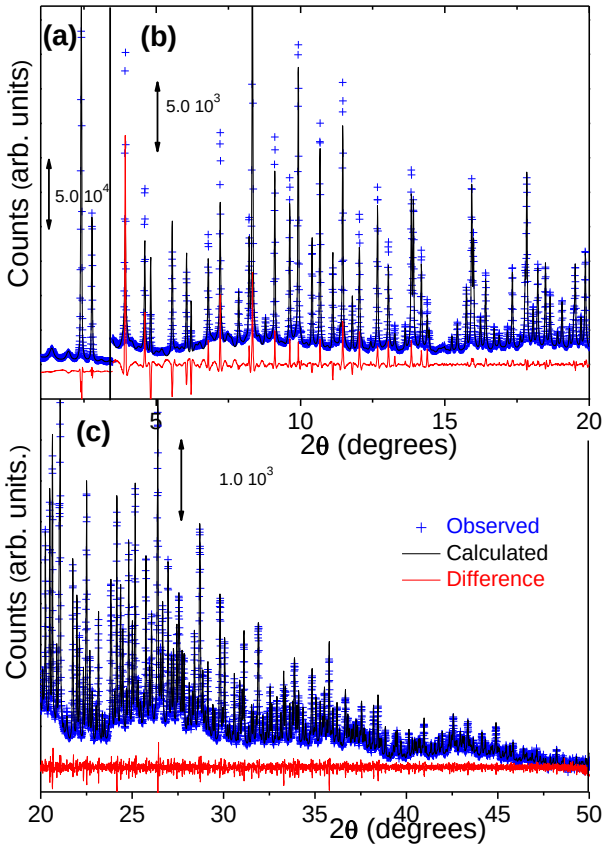

Fig. 2. HR-XRPD data collected at RT on the solvated sample at ESRF BM01B (blue crosses), Rietveld refinement (superimposed black full line) and residual (vertically shifted red full line). λ= 0. 50114(4).

The initial structural model was based on the published model for Zr-UiO-66.[56] Some broad peaks thought to be due to impurities were first modeled as single peaks with refined intensities. The first Rietveld refinement of the framework gave a good fit with R_{wp} = 14.636. During this refinement we refined the background, zero point, scale and peak broadening as well as isotropic thermal parameters for oxygen and hafnium, in addition to the refinement of hafnium coordinates. Attempts to refine the carbon and oxygen coordinates led to divergence. Because of HR-XRPD data of very high quality we were able to use difference Fourier maps to identify a hydrogen bonded oxygen atom (O3) from a solvent water molecule situated close to O2 (O2-O3 = 2.093 Å). Subsequent difference Fourier maps allowed the location of two further atom positions assigned to diffuse electron density from solvent molecules in the pores. The occupancy parameters of all the non framework atoms were refined.

To better understand the origin for the weak broad peaks (the most intense being seen at 2θ ≈ 2.0 and 1.4 degrees in Fig. 2a, also visible in the red pattern of Fig. 1a), a second refinement was carried out in TOPAS academic using a combined Rietveld[76] and Pawley[81] model. This allowed fitting of the broad peaks from the primitive superstructure of UiO-66. The output of the first Rietveld model was used as a starting point for the final combined refinement. The Pawley model was a primitive cubic unit cell (space group *Pm*-3*m*, no. 221) with the lattice parameter constrained to be the same as that of the Rietveld model. Separate peak broadening parameters were refined for the two models to account for the differences in peak shape between the peaks from the normal centered cell and the primitive super cell.

Four background parameters, zero and adsorption corrections were refined for the overall pattern. The face-centered Rietveld model had 7 structural parameters, scale and Gaussian and Lorentzian particle size broadening parameters. The primitive cubic model for the Pawley

refinement used the same lattice parameter and a Lorentzian particle size broadening term. Final R values: r_{wp} = 9.553; r_{exp} = 1.130; r_p = 6.446; GoF = 8.450. R_{Bragg} values were 5.893 for the Rietveld phase and 1.057 for the Pawley phase. The quality of the refinement can be appreciated in Fig. 2 and Fig. 3, the former reporting the full refined 2θ range, the latter (reporting a shorter angular range) includes tick-marks for the two phases included in refinement (*Fm*-3*m* and *Pm*-3*m*). The details of the final refinement are given in Table 3 and coordinates are given in Table 4. Numerical results obtained from the combined Rietveld-Pawley are almost equivalent (within e.s.d.) to those obtained from the previous Rietveld refinement.

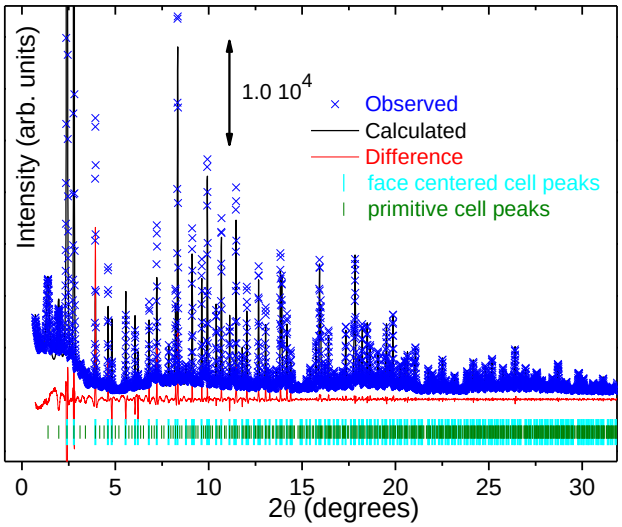

Fig. 3. Observed (scattered crosses), calculated (black line) and difference (red line) plots for the final combined Rietveld-Pawley refinement of solvated Hf-UiO-66. λ = 0.50114(4) Å. Note that the large main two peaks, view in the low 2θ region, are truncated to better display the fit on the weaker peaks at higher 2θ. See Fig. 2a to appreciate the relative intensities. Predicted peak positions for the face centered and primitive cells are shown with cyan and green dashes respectively.

Table 3. Final Rietveld-Pawley refinement: coordinates, site occupancies and thermal parameters for the solvated Hf-UiO-66. Parameters without ESDs were not refined.

Compound formula	$Hf_{24}O_{120}C_{192}H_{96}$
Crystal system	Cubic
Space group	*Fm*-3*m* (No. 225)
a, *b*, *c* (Å)	20.7006(3)
volume (Å^3)	8870.5(4)
Instrument	SNBL station BM10B. Two-circle diffractometer with 6 counting chains.
λ (Å)	0.50114(4)
Collection temperature (°C)	24
R_{wp}, R_p, R_{exp}	9.413, 6.757, 1.130
χ^2	8.327
2θ range (degree)	0.7 - 50
Parameters (Rietveld)	16
Constraints	0

Determining a structure from the broad peaks of the primitive supercell was not possible, however, by linking the unit cells of the two models we demonstrate that the two phases are related. The broad peaks are neatly fitted by a primitive supercell with the same cell parameter as the face-centered Rietveld cell. We believe the extra broadening of the supercell peaks is due to partial occupancy of the voids in the structure with ordered solvent molecules; the remaining voids are either empty or occupied by disordered solvent. We believe that these inconsistencies cause a degree of strain in the crystal lattice (some voids are expanded as they are occupied by solvent while their neighbors are not) which leads to additional peak broadening in the supercell. Dummy carbon atoms were used in the Rietveld model to account for the electron density from the

disordered solvent, as already done in the initial Rietveld refinement. The poorly fitted peak intensity at 2θ = 3.9 degree is probably due to disordered solvent not accounted for by the dummy carbon atoms. Linker atom positions were not refined.

Table 4. Fractional coordinates, site occupancies and thermal parameters for solvated Hf-UiO-66. Parameters without ESDs were not refined. $a = b = c = 20.7006(3)$ Å^3.

Site	x	y	z	Occupancy	Biso (Å^2)
Hf1	0.11988(8)	0	0	1	0.97(3)
O1	0.1675	0	0.0888	1	2.3(3)
O2	0.0556(8)	-0.0556(8)	-0.0556(8)	1	2.3(3)
C11	0.149	0	-0.149	1	1.5
C12	0.2007	0	0.2007	1	1.5
C13	0.2668	0	0.1849	1	1.5
H1	0.3683	0	0.2198	1	1.7
O3	0.61744	0.88256	0.38256	0.27(2)	2.5
C1	0.56193	0.93807	0.93807	0.28(3)	1.5
C2	0	0	0.37456	0.33(3)	1.5

The high quality of the synchrotron XRPD data revealed though Rietveld-Pawley refinement new insight on the surroundings around the metal clusters in the MOF. Fig. 4 shows a water molecule strongly hydrogen bonded in a very specific position on the outside of the Hf cluster in a position previously unknown for the Zr-UiO-MOF series.[56,80]

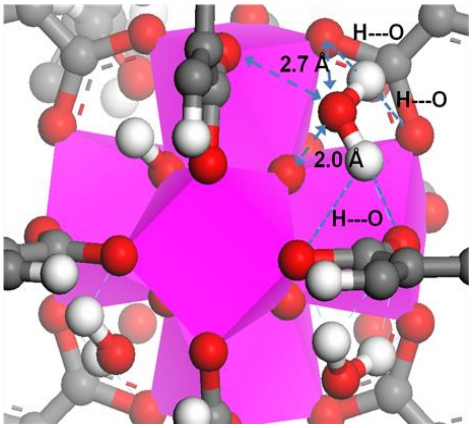

Fig. 4. Distances between the solvent water molecule and its closest neighboring O atoms. Color scheme: Hf cluster coordination sphere (purple), O (red), C (grey), H (white).

2. In situ HR-XRPD study of desolvation

The thermal resistance of Hf-UiO-66 was further investigated by *in situ* XRPD (Fig. 5a) and EXAFS (see Section III.B.3) using synchrotron radiation. As already usefully done for other temperature dependent XRPD studies on porous materials,[74,75,82] XRPD data were refined to determine structure changes during the thermal gradient. XRPD showed a clear change in unit cell parameters and in electron density in the MOFs pores during heating, interpreted as a combination of loosely coordinated solvent molecules initially loosing coordination and then leaving the structure, both averaging and lowering electron density. From the TGA-MS data it is clear that after an initial small loss of solvent (water) around 100 °C, the bulk inclusion in the pores (25 mass % of the inactivated MOF, DMF) was removed between 150 and 250 °C (Table 1 and Fig. 1b). Both XRPD and TGA showed the very high thermal stability, already observed the UiO zirconium series, with crystallinity intact even at 400 °C.

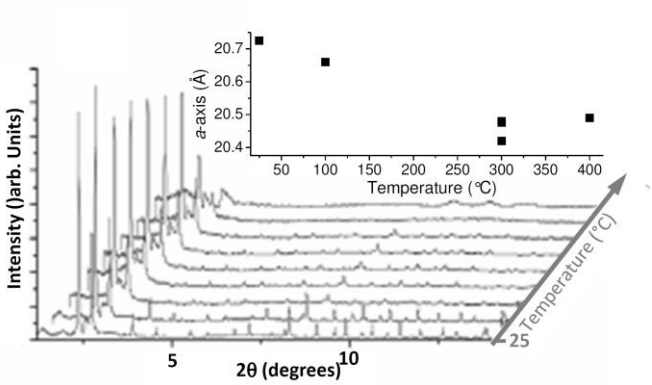

Fig. 5. Selection of raw XRPD patterns collected as a function of the temperature. λ = 0.50114(4) Å. Inset: refined *a*-axis length of Hf-UiO-66 plotted against temperature in the temperature resolved HR-XRPD experiment performed in situ at BM01B beamline of the ESRF synchrotron. An isotherm step was done at 300 °C allowing the collection of there successive patterns.

HR-XRPD patterns of crystalline Hf-UiO-66were collected as a function of the temperature (25, 100, 300 and 400 °C), in a shorter angular range (1.2 degree < 2θ < 25 degree). Pattern collected at 500 and 600 °C testified the first stages of the amorphization process and the successive structure collapse, respectively, in agreement with TGA data(Fig. 1b). The data collected in the 25–400 °C interval were refined using the Rietveld method with the model obtained above (Table 3 and Table 4) in TOPAS academic[83] to obtain unit cell parameter. The occupancy of the solvent related sites C1 and C2 were also refined. The occupancies of these sites were found to drop to zero above 100 °C. The powder pattern changes significantly above 100 °C (Fig. 5) and this corresponds to a significant reduction in the unit cell edge length *a* (inset in Fig. 5). While the temperature is held at 300 °C *a* increases slightly, but is further reduced at 400 °C. These data represents a further evidence of the negative thermal expansion already observed from other MOFs materials such as MOF-5,[84-86] MOF-C22,[87] and CPO-27-Ni.[88,89]

3. In situ EXAFS study of desolvation

For the determination of complex MOFs structure, the combined use of XRPD and EXAFS has been demonstrated to be a powerful structural elucidation tool when single crystal data are not available.[56,70,88-99] In some cases also the pair distribution function approach has been adopted.[100] Where XRPD data mainly provides topological information, Hf L_3-edge EXAFS data reveal details about the immediate surroundings of the Hf atoms. The Fourier transform (FT) of the EXAFS signal for the Hf-UiO-66 measured at room temperature and at 300 °C are reported in Fig. 6 (cyan and orange spectra), superimposed with the corresponding best fits (blue and red spectra) performed using as input the structures optimized by XRPD and following the same refinement strategy already successfully used to optimize the Zr-homologue of UiO-66.[56,70]

Both moduli and imaginary parts show, upon thermal activation, a shift toward lower R-values of the first shell and of the contributions in the range between 2 and 3 Å (phase uncorrected), thus validating the general shortening of distances, when temperature is raised, found by XRPD analysis (Fig. 5b). It is also evident a considerable decrease of the signal around 3.4 Å, assignable to the Hf-Hf contribution. This is only partially due to an increase of the thermal disorder, but is mainly due by the fact that the activation causes a significant distortion of the Hf_6 octahedron resulting in two significantly different Hf-Hf distances, which contributions interfere destructively (see the corresponding imaginary parts in the inset of Fig. 6). EXAFS refinements result in the structural model for Hf-UiO-66 reported in Fig. 4, where also the distances obtained from the XRPD refinement are reported for comparison..

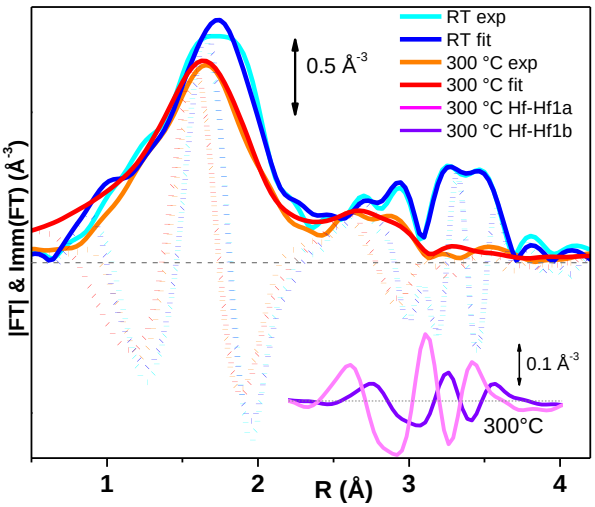

Fig. 6. k^2-weighted, phase uncorrected FT of the Hf L_3-edge EXAFS spectra HF-UiO-66 sample in its solvated (cyan) and desolvated (orange) forms (see SI for the experimental set-up). Modulus and imaginary parts are reported as full and dotted lines, respectively. Blue and red curves reports the corresponding best fits.

Table 5. Summary of the parameters optimized in the fitting of the EXAFS data (Fig. 6 and Fig. 7) on the Hf-UiO-66 sample measured at room temperature and at 300°C. A single ΔE_0 and a single S_0^2 have been optimized for all SS and MS paths according to the procedure described elsewhere.[80] Optimized bond distances are compared to the values obtained from XRPD refinement. For each path contributing to the EXAFS signal, also the degeneration path (N) is reported. As deeply discussed in Ref. [80] for symmetry reasons this degeneration may be different from that used in the XRPD refinement (also reported in the Table).

	Solvated Hf-UiO-66		Desolvated Hf-UiO-66	
Collection T (°C)	30		300	
	EXAFS	XRPD	EXAFS	XRPD
R-factor	0.019	-	0.050	-
S_0^2	0.91 ± 0.06	-	0.91	-
ΔE_0 (eV)	2.2 ± 0.6	-	2.4 ± 0.7	-
$R_{\mu 3O}$ (Å)	2.12 ± 0.01 (N=2)	2.082 (N=4)	2.06 ± 0.01 (N=3)	2.068 (N=4)[a]
R_O (Å)	2.25 ± 0.01 (N=6)	2.150 (N=4)	2.19 ± 0.01 (N=4)	2.115 (N=4)
σ^2_O (Å^2)	0.005 ± 0.002	-	0.009 ± 0.002	-
R_C (Å)	3.23 ± 0.06 (N=4)	3.144 (N=4)	3.22 ± 0.05 (N=4)	3.113 (N=4)
σ^2_C (Å^2)	0.014 ± 0.011		0.016 ± 0.013	-
R_{Hf1a} (Å)	3.510 ± 0.005 (N=4)	3.533 (N=4)	3.31 ± 0.03 (N=8/3)	3.466 (N=4)
R_{Hf1b} (Å)	degenerate with R_{Hf1a}	-	3.45 ± 0.06 (N=4/3)	-
σ^2_{Hf1} (Å^2)	0.0042 ± 0.0004	-	0.009 ± 0.004	-
R_{Hf2} (Å)	4.964 (N=1)[b]	4.996 (N=1)	below noise level	4.902 (N=1)
σ^2_{Hf} (Å^2)	0.008 ± 0.002	-	below noise level	-

[a] Degeneration of 4, with occupancy factor fixed to 0.75, resulting in an average stoichiometry of 3 μ3-O ligand per Hf atom.

[b] Distance optimized non independently according to the geometrical constrain coming form a perfect Hf_6 octahedron: $R_{Hf2} = \sqrt{2}\, R_{Hf1}$. After propagation, the corresponding error is 0.007 Å.

The results of the data fit are reported in Table 5 For the as-synthesized sample, the R-factor of 0.019 confirms the good agreement between the fit and experimental data already appreciable in Fig. 7a,b. Amplitude and energy shift values obtained are physically meaningful; in general all the optimized distances are slightly longer than the ones extracted from XRPD data (Table 5). The optimized values for the Debye-Waller factors of oxygen and hafnium are proportioned to the distance from the absorber and to the number of electrons of the scattering atoms, for the same

reason errors related to Hf-Hf_1 path are low. Only the value for the carbon atoms is a bit higher than expected and has also an higher related error; this is due to the difficulty in isolating the signal of Hf-C path because in the involved R-range there are many other path contributions as deeply discussed elsewhere[80] for the Zr-UiO-66 homologue.

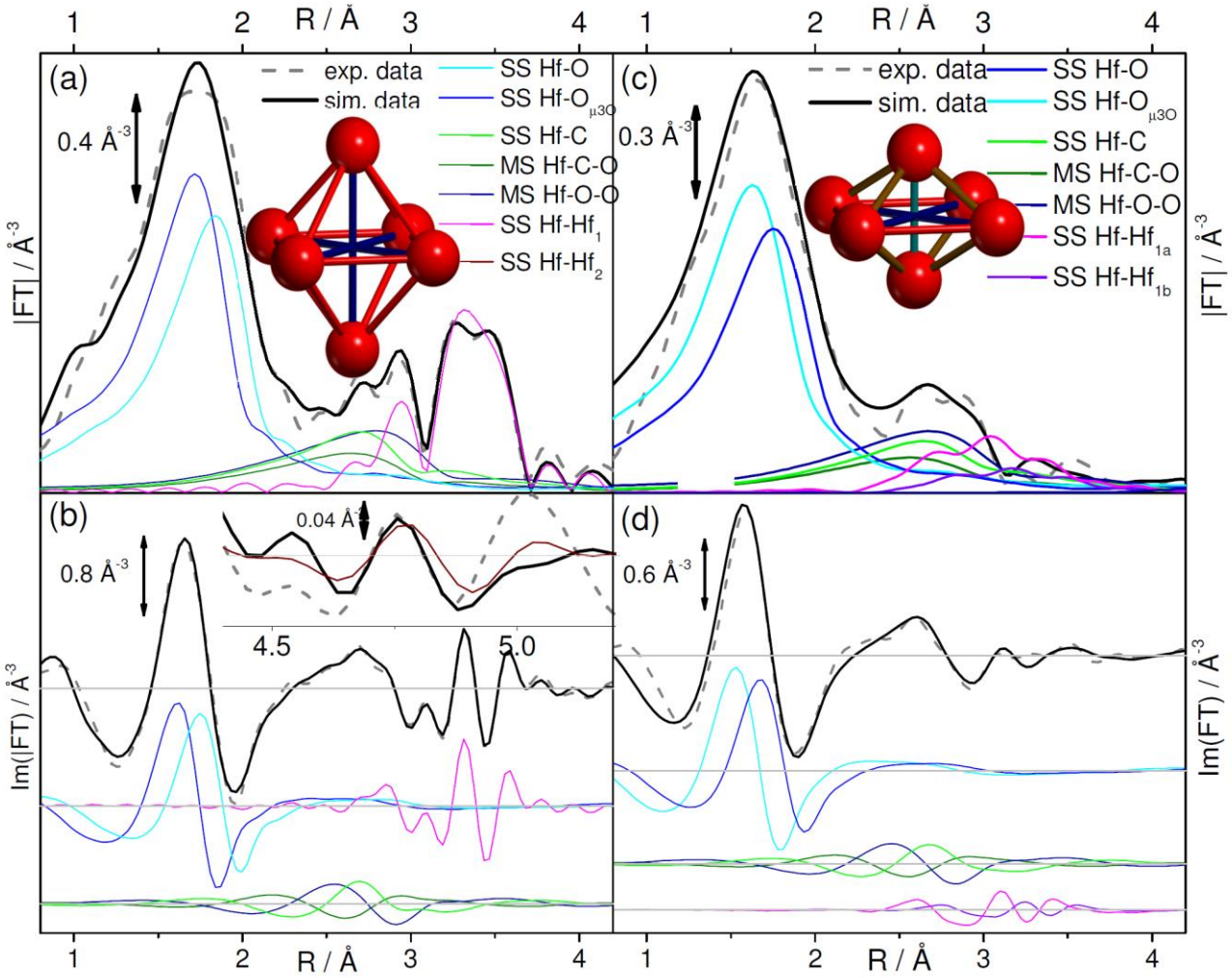

Fig. 7. Comparison between experimental (dashed grey curves) and corresponding best fits (solid black lines) and contributions from the most important paths for Hf-UiO-66 measured at room temperature, parts (a) and (b) and at 300 °C, parts (c) and (d). Parts (a,c) and (b,d) reports the modulus and the imaginary parts, respectively. The inset of part (b) is a magnification of the region at high R where the contribution of diagonal Hf occurs (Hf-Hf_2 path). For quantitative values of the parameters optimized in the fits, see Table 5. The structural models in parts (a) and (c) reports the perfect octahedron $Hf_6(OH)_4O_4$ and the squeezed Hf_6O_6 octahedron (only Hf atoms being reported for clarity) used to model the Hf-Hf_1 and Hf-Hf_2 distances in the solvated (RT data) and desolvated (300 °C data) forms of Hf-UiO-66.

The data analysis of the Hf-MOF sample measured after heating at 300 °C was performed following a similar procedure, all the paths described previously remained almost unchanged. Only for the Hf-Hf_1 SS path a different model was used. On the basis of what already learnt from the Zr-UiO-66 homologue[80] and considering that the signal at around 3.4 Å in the FT of the data is much lower, we hypothesized that the perfect octahedral metal center underwent a slight deformation. Indeed, the inorganic cornerstone of the material measured at RT is a perfect $Hf_6(OH)_4O_4$ octahedron (see model in Fig. 7a), with 6 equivalent Hf at the vertex, 12 equivalent Hf-Hf_1 sides and 3 equivalent and Hf-Hf_2 diagonals. Upon desolvation (sample measured at 300 °C) 2 structural water molecules are lost per cornerstone unit, that evolves from $Hf_6(OH)_4O_4$ to Hf_6O_6.[70,80] The new Hf_6O_6 octahedron compressed (2 opposite vertexes approaching, see model in Fig. 7c) resulting in the shortening of 8 of the 12 edges, and the elongation of the other 4 edges. To take into account this variation we simulated the EXAFS contribution with two independently parameterized paths

fixing for the degeneration a ratio of 1/3 and 2/3 with respect to the case of the single contribution. The structural changes of the Hf_6 octahedron occurring upon desolvation is graphically represented by the evolution of the two models reported in parts (a) and (c) of Fig. 7.

We decided to fix the S_0^2 parameter to the value obtained for the same system at room temperature. In this way the total number of fit parameters remains constant. The comparison between experimental and simulated curves is shown in Fig. 7c,d. The results obtained are reported in the fourth column of Table 5 and they confirm the general shortening of the distances, after increasing the temperature, observed by XRPD and by a qualitative observation of the raw EXAFS data in R space (Fig. 6). The fit effectively found a minimum with two different lengths for Hf-Hf_1 paths and the fact that shorter distances are 2/3 of the total indicates that the octahedral metal centre underwent a contraction. A further confirmation comes by the lower optimized value of the opposite Hf distance. Moreover, it is worth to notice that all Debye-Waller factors are higher with respect to the previous data analysis. This can be explained by an increasing of the motion of the atoms with respect to their average position due to the raising of the temperature.

C. Potential application of Hf-UiO-66 and B-functionalized UiO-66 as scavengers for radioactive wastes

We have presented here a thorough investigation of a new hafnium-containing MOF, Hf-UiO-66, with the same topology and thermal stability as the Zr-UiO-66 MOF (Fig. 1b and Fig. 5a) but with the added potential for uses within radiation hosting, scavenging and protecting. Indeed, zirconium (Z=40) has a medium stopping power for electromagnetic radiation and charged particles (α, p^+, p^-, e^-, e^+) but a poor neutron absorption cross section (σ_{abs} = 0.185(3) barn: 1 barn = 10^{-28} m^2)[71] and the same is true for the organic part of this MOF (σ_{abs} = 0.00350(7), 1.90(3) and 0.00019(2) barn for C, N and O, nuclei respectively).[71] Fortunately hafnium, which has chemistry very similar to zirconium, is a very good absorber of both neutrons (σ_{abs} = 104.1(5) barn)[71] and electromagnetic radiation and charged particles (Z = 72). Differently to what's observed form other MOFs materials, the UiO-66 framework exhibits also a remarkable stability against external mechanical pressure: XRPD testified that UiO-66 maintains crystallinity up to the maximum investigated pressure of 10^8 Pa.[56] A remarkable stability was also observed after interaction with the standard solvents such as water, acetone, benzene, ethanol and DMF as well after interaction aggressive acid (HCl) and basic (NaOH) conditions.[56,80]

Finally, to further improve this MOF system further towards neutron emitting radioactive waste scavenging, the radiation absorption properties of the linkers have to be improved. Regular organic compounds (in our case organic dicarboxylates, see Fig. 8d) do not have any significant radiation absorption properties (see above). The only element with carbon-like bonding properties and remarkably high neutron absorption is boron (σ_{abs} = 767(8) barn).[71] The *p*-carborane closely resembles a benzene ring and has already been employed as its dicarboxylate (see Fig. 8c) in MOF chemistry where a MOF-5 type material incorporating this linker was made.[73] Preliminary work with *p*-carborane dicarboxylic acid and zirconium has already furnished the *p*-carborane equivalent of Zr-UiO-66 (Fig. 8a); the material showed a good crystallinity, as testified by the pattern reported in see Fig. 8b (blue curve). We currently work to optimize the synthesis protocol before turning to the more expensive and essential Hf equivalent. The resulting four systems will represent a significant improvement for the class of microporous materials towards intermediate nuclear waste scavenging and radiation protection.

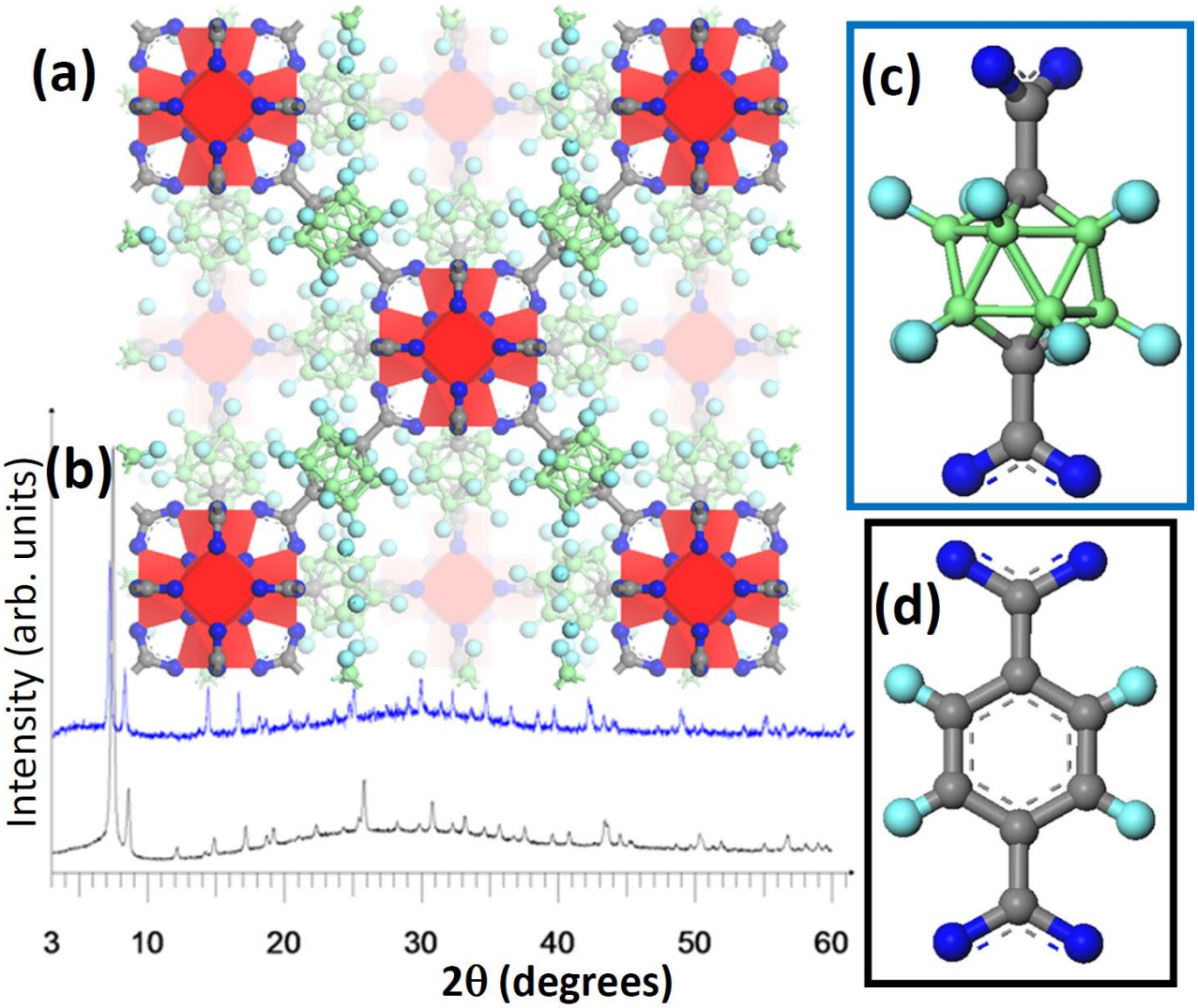

Fig. 8. Part (a): the *p*-carborane-dicarboxylate version of the Zr-UiO-66. Color scheme: Zr coordination sphere (red) , O (blue), C (grey), B (green), H (turquoise). Part (b): XRPD patterns of the p-carborane equivalent of Zr-UiO-66 (blue) and Zr-UiO-66 itself (black). λ = 1.540 Å. Parts (c) and (d): linkers of the *p*-carborane-dicarboxylate version of the Zr-UiO-66 and of Zr-UiO-66, respectively. Color code as in part (a).

IV. CONCLUSIONS

In this work we have reported a thorough investigation of a new hafnium-containing MOF, Hf-UiO-66, with the same topology and thermal stability as the Zr-UiO-66 MOF. The high internal surface area of the UiO-66 framework, together with its remarkable resistance to temperature (framework breakdown observed at 500 °C), pressure (no collapse observed up to 10^8 Pa), and chemical aggressions makes the UiO-66 structure of potential interest for the interim storage of radioactive waste. The remarkable advantage of the Hf- and B-functionalized UiO-66 class of MOFs with respect the other microporous materials used so far for this purpose (silica aerogels[53] and zeolites[54,55]) is evident.

According to the recent study of the Lin group,[72] Hf-UiO-66 is certainly interesting application as contrast agent for computed tomography imaging inside living tissues.

ACKNOWLEDGMENTS

The authors thank S. Aravinthan for performing the TGA-MS measurements, J. T. Hupp for access to *p*-carborane-dicarboxylic acid, Swiss Norwegian Beamlines (SNBL) at ESRF, Grenoble,

France for synchrotron beam time and FUNMAT@UIO, inGAP, VISTA, The Research Council of Norway and *Progetti di Ricerca di Ateneo -Compagnia di San Paolo- 2011-linea A1, progetto ORTO11RRT5* for financial support.

---

* carlo.lamberti@unito.it

[1]G. Ferey and C. Serre *Chem. Soc. Rev.* **38**, 1280 (2009).
[2]J. R. Long and O. M. Yaghi *Chem. Soc. Rev.* **38**, 1213 (2009).
[3]N. Stock and S. Biswas *Chem. Rev.* **112**, 933 (2012).
[4]S. M. Cohen *Chem. Rev.* **112**, 970 (2012).
[5]H. Furukawa, N. Ko, Y. B. Go, N. Aratani, S. B. Choi, E. Choi, A. O. Yazaydin, R. Q. Snurr, M. O'Keeffe, J. Kim and O. M. Yaghi *Science* **329**, 424 (2010).
[6]A. Czaja, T. Trukhan and U. Müller *Chem. Soc. Rev.* **38**, 1284 (2009).
[7]T. Yildirim and M. R. Hartman *Phys. Rev. Lett.* **95**, 215504 (2005).
[8]I. Cabria, M. J. Lopez and J. A. Alonso *Phys. Rev. B* **78**, 205432 (2008).
[9]S. A. FitzGerald, K. Allen, P. Landerman, J. Hopkins, J. Matters, R. Myers and J. L. C. Rowsell *Phys. Rev. B* **77**, 224301 (2008).
[10]J. G. Vitillo, L. Regli, S. Chavan, G. Ricchiardi, G. Spoto, P. D. C. Dietzel, S. Bordiga and A. Zecchina *J. Am. Chem. Soc.* **130**, 8386 (2008).
[11]L. Z. Kong, G. Roman-Perez, J. M. Soler and D. C. Langreth *Phys. Rev. Lett.* **103**, 096103 (2009).
[12]L. J. Murray, M. Dinca and J. R. Long *Chem. Soc. Rev.* **38**, 1294 (2009).
[13]S. A. FitzGerald, J. Hopkins, B. Burkholder, M. Friedman and J. L. C. Rowsell *Phys. Rev. B* **81**, 104305 (2010).
[14]L. Z. Kong, Y. J. Chabal and D. C. Langreth *Phys. Rev. B* **83**, 121402 (2011).
[15]K. Sumida, D. L. Rogow, J. A. Mason, T. M. McDonald, E. D. Bloch, Z. R. Herm, T. H. Bae and J. R. Long *Chem. Rev.* **112**, 724 (2012).
[16]J.-R. Li, R. J. Luppler and H. C. Zhou *Chem. Soc. Rev.* **38**, 1477 (2009).
[17]J. R. Li, J. Sculley and H. C. Zhou *Chem. Rev.* **112**, 869 (2012).
[18]K. A. Cychosz, R. Ahmad and A. J. Matzger *Chem. Sci.* **1**, 293 (2010).
[19]B. Xiao, P. S. Wheatley, X. B. Zhao, A. J. Fletcher, S. Fox, A. G. Rossi, I. L. Megson, S. Bordiga, L. Regli, K. M. Thomas and R. E. Morris *J. Am. Chem. Soc.* **129**, 1203 (2007).
[20]P. Horcajada, R. Gref, T. Baati, P. K. Allan, G. Maurin, P. Couvreur, G. Ferey, R. E. Morris and C. Serre *Chem. Rev.* **112**, 1232 (2012).
[21]A. Corma, H. Garcia and F. X. L. Xamena *Chem. Rev.* **110**, 4606 (2010).
[22]M. Yoon, R. Srirambalaji and K. Kim *Chem. Rev.* **112**, 1196 (2012).
[23]L. E. Kreno, K. Leong, O. K. Farha, M. Allendorf, R. P. Van Duyne and J. T. Hupp *Chem. Rev.* **112**, 1105 (2012).
[24]H. Kitagawa, Y. Nagao, M. Fujishima, R. Ikeda and S. Kanda *Inorg. Chem. Commun.* **6**, 346 (2003).
[25]J. C. G. Bunzli and C. Piguet *Chem. Rev.* **102**, 1897 (2002).
[26]S. Bordiga, C. Lamberti, G. Ricchiardi, L. Regli, F. Bonino, A. Damin, K. P. Lillerud, M. Bjorgen and A. Zecchina *Chem. Commun.*, 2300 (2004).
[27]M. D. Allendorf, C. A. Bauer, R. K. Bhakta and R. J. T. Houk *Chem. Soc. Rev.* **38**, 1330 (2009).
[28]M. Kurmoo *Chem. Soc. Rev.* **38**, 1353 (2009).
[29]C. G. Silva, A. Corma and H. Garcia *J. Mater. Chem.* **20**, 3141 (2010).
[30]M. Mattesini, J. M. Soler and F. Yndurain *Phys. Rev. B* **73**, 094111 (2006).
[31]J. C. Tan, B. Civalleri, C. C. Lin, L. Valenzano, R. Galvelis, P. F. Chen, T. D. Bennett, C. Mellot-Draznieks, C. M. Zicovich-Wilson and A. K. Cheetham *Phys. Rev. Lett.* **108**, 095502 (2012).
[32]C. Chmelik, H. Bux, J. Caro, L. Heinke, F. Hibbe, T. Titze and J. Kaerger *Phys. Rev. Lett.* **104**, 085902 (2010).
[33]N. Tsoulfanidis and R. G. Cochran *Nucl. Technol.* **93**, 263 (1991).
[34]R. L. Keeney and D. Vonwinterfeldt *Risk Anal.* **14**, 107 (1994).
[35]P. Slovic, J. H. Flynn and M. Layman *Science* **254**, 1603 (1991).
[36]R. P. Rechard *Reliab. Eng. Syst. Saf.* **69**, 5 (2000).
[37]D. Streimikiene and A. Mikalauskiene *Renew. Sust. Energ. Rev.* **14**, 1600 (2010).
[38]D. Neff, M. Saheb, J. Monnier, S. Perrin, M. Descostes, V. L'Hostis, D. Crusset, A. Millard and P. Dillmann *J. Nucl. Mater.* **402**, 196 (2010).
[39]R. C. Ewing, W. J. Weber and J. Lian *J. Appl. Phys.* **95**, 5949 (2004).
[40]B. Made, A. Clement and B. Fritz *Comput. Geosci.* **20**, 1347 (1994).
[41]M. J. O'Sullivan, K. Pruess and M. J. Lippmann *Geothermics* **30**, 395 (2001).
[42]A. Gens *Geotechnique* **60**, 3 (2010).
[43]A. Macfarlane *Annu. Rev. Energ. Environ.* **26**, 201 (2001).
[44]L. W. Hobbs, F. W. Clinard, S. J. Zinkle and R. C. Ewing *J. Nucl. Mater.* **216**, 291 (1994).
[45]O. Terra, N. Clavier, N. Dacheux and R. Podor *New J. Chem.* **27**, 957 (2003).
[46]J. M. Montel, B. Glorieux, A. M. Seydoux-Guillaume and R. Wirth *J. Phys. Chem. Solids* **67**, 2489 (2006).

[47]G. R. Lumpkin *Elements* **2**, 365 (2006).
[48]W. J. Weber, A. Navrotsky, S. Stefanovsky, E. R. Vance and E. Vernaz *MRS Bull.* **34**, 46 (2009).
[49]K. A. H. Kubatko, K. B. Helean, A. Navrotsky and P. C. Burns *Science* **302**, 1191 (2003).
[50]A. D. Handoko and G. K. L. Goh *Sci. Adv. Mater.* **2**, 16 (2010).
[51]P. P. Bose, R. Mittal and S. L. Chaplot *Phys. Rev. B* **79**, 174301 (2009).
[52]H. Matzke and E. Vernaz *J. Nucl. Mater.* **201**, 295 (1993).
[53]P. R. Aravind, L. Sithara, P. Mukundan, P. K. Pillai and K. G. K. Warrier *Mater. Lett.* **61**, 2398 (2007).
[54]J. D. Sherman *Proc. Natl. Acad. Sci. USA* **96**, 3471 (1999).
[55]C. Sanchez-Valle, C. H. Chio and G. D. Gatta *J. Appl. Phys.* **108**, 093509 (2010).
[56]J. H. Cavka, S. Jakobsen, U. Olsbye, N. Guillou, C. Lamberti, S. Bordiga and K. P. Lillerud *J. Am. Chem. Soc.* **130**, 13850 (2008).
[57]C. G. Silva, I. Luz, F. X. Llabres i Xamena, A. Corma and H. Garcia *Chem.-Eur. J.* **16**, 11133 (2010).
[58]S. J. Garibay and S. M. Cohen *Chem. Commun.* **46**, 7700 (2010).
[59]V. Guillerm, S. Gross, C. Serre, T. Devic, M. Bauer and G. Ferey *Chem. Commun.* **46**, 767 (2010).
[60]M. Kandiah, S. Usseglio, S. Svelle, U. Olsbye, K. P. Lillerud and M. Tilset *J. Mater. Chem.* **20**, 9848 (2010).
[61]K. P. Lillerud, U. Olsbye and M. Tilset *Top. Catal.* **53**, 859 (2010).
[62]S. Chavan, J. G. Vitillo, M. J. Uddin, F. Bonino, C. Lamberti, E. Groppo, K. P. Lillerud and S. Bordiga *Chem. Mat.* **22**, 4602 (2010).
[63]M. Kandiah, M. H. Nilsen, S. Usseglio, S. Jakobsen, U. Olsbye, M. Tilset, C. Larabi, E. A. Quadrelli, F. Bonino and K. P. Lillerud *Chem. Mat.* **22**, 6632 (2010).
[64]F. Vermoortele, R. Ameloot, A. Vimont, C. Serre and D. De Vos *Chem. Commun.* **47**, 1521 (2011).
[65]M. Kim, J. A. Boissonnault, P. V. Dau and S. M. Cohen *Angew. Chem.-Int. Edit.* **50**, 12193 (2011).
[66]A. Schaate, P. Roy, A. Godt, J. Lippke, F. Waltz, M. Wiebcke and P. Behrens *Chem.-Eur. J.* **17**, 6643 (2011).
[67]Q. Y. Yang, H. Jobic, F. Salles, D. Kolokolov, V. Guillerm, C. Serre and G. Maurin *Chem.-Eur. J.* **17**, 8882 (2011).
[68]C. Wang, Z. G. Xie, K. E. deKrafft and W. L. Lin *J. Am. Chem. Soc.* **133**, 13445 (2011).
[69]M. Kim, J. F. Cahill, Y. X. Su, K. A. Prather and S. M. Cohen *Chem. Sci.* **3**, 126 (2012).
[70]S. Chavan, J. G. Vitillo, D. Gianolio, O. Zavorotynska, B. Civalleri, S. Jakobsen, M. H. Nilsen, L. Valenzano, C. Lamberti, K. P. Lillerud and S. Bordiga *Phys. Chem. Chem. Phys.* **14**, 1614 (2012).
[71]Values for thermal neutrons (v = 2200 m/s), taken from V. F. Sears, Neutron News, **3/3**, 26 (1992), also available on line at http//www.ncnr.nist.gov/resources/n-lengths/.
[72]W. Lin, K. deKrafft, W. Boyle, L. Burk and O. Zhou *J. Mater. Chem.* **22**, DOI: 10.1039/C2JM32299D (2012).
[73]O. K. Farha, A. M. Spokoyny, K. L. Mulfort, M. F. Hawthorne, C. A. Mirkin and J. T. Hupp *J. Am. Chem. Soc.* **129**, 12680 (2007).
[74]M. Milanesio, G. Artioli, A. F. Gualtieri, L. Palin and C. Lamberti *J. Am. Chem. Soc.* **125**, 14549 (2003).
[75]G. Agostini, C. Lamberti, L. Palin, M. Milanesio, N. Danilina, B. Xu, M. Janousch and J. A. van Bokhoven *J. Am. Chem. Soc.* **132**, 667 (2010).
[76]H. M. Rietveld *Acta Crystallogr.* **22**, 151 (1967).
[77]A. A. Coelho, J. Appl. Crystallogr., **38**, 455 (2005); TOPAS V4.1, Bruker AXS, (2006).
[78]B. Ravel and M. Newville *J. Synchrot. Radiat.* **12**, 537 (2005).
[79]A. L. Ankudinov, A. I. Nesvizhskii and J. J. Rehr *Phys. Rev. B* **67**, Art. No. 115120 (2003).
[80]L. Valenzano, B. Civalleri, S. Bordiga, M. H. Nilsen, S. Jakobsen, K.-P. Lillerud and C. Lamberti *Chem. Mater.* **23**, 1700 (2011).
[81]G. Pawley *J. Appl. Cryst.* **14**, 357 (1981).
[82]D. S. Wragg, D. Akporiaye and H. Fjellvag *J. Catal.* **279**, 397 (2011).
[83]A. A. Coelho *J. Appl. Crystallogr.* **38**, 455 (2005).
[84]D. Dubbeldam, K. S. Walton, D. E. Ellis and R. Q. Snurr *Angew. Chem.-Int. Edit.* **46**, 4496 (2007).
[85]W. Zhou, H. Wu, T. Yildirim, J. R. Simpson and A. R. H. Walker *Phys. Rev. B* **78**, 054114 (2008).
[86]N. Lock, Y. Wu, M. Christensen, L. J. Cameron, V. K. Peterson, A. J. Bridgeman, C. J. Kepert and B. B. Iversen *J. Phys. Chem. C* **114**, 16181 (2010).
[87]S. S. Han and W. A. Goddard *J. Phys. Chem. C* **111**, 15185 (2007).
[88]S. Bordiga, F. Bonino, K. P. Lillerud and C. Lamberti *Chem. Soc. Rev.* **39**, 4885 (2010).
[89]L. Valenzano, J. G. Vitillo, S. Chavan, B. Civalleri, F. Bonino, S. Bordiga and C. Lamberti *Catal. Today* **182**, 67 (2012).
[90]C. Prestipino, L. Regli, J. G. Vitillo, F. Bonino, A. Damin, C. Lamberti, A. Zecchina, P. L. Solari, K. O. Kongshaug and S. Bordiga *Chem. Mat.* **18**, 1337 (2006).
[91]K. C. Szeto, K. P. Lillerud, M. Tilset, M. Bjorgen, C. Prestipino, A. Zecchina, C. Lamberti and S. Bordiga *J. Phys. Chem. B* **110**, 21509 (2006).
[92]K. C. Szeto, C. Prestipino, C. Lamberti, A. Zecchina, S. Bordiga, M. Bjorgen, M. Tilset and K. P. Lillerud *Chem. Mater.* **19**, 211 (2007).
[93]J. Hafizovic, M. Bjorgen, U. Olsbye, P. D. C. Dietzel, S. Bordiga, C. Prestipino, C. Lamberti and K. P. Lillerud *J. Am. Chem. Soc.* **129**, 3612 (2007).

[94]F. Bonino, S. Chavan, J. G. Vitillo, E. Groppo, G. Agostini, C. Lamberti, P. D. C. Dietzel, C. Prestipino and S. Bordiga *Chem. Mater.* **20**, 4957 (2008).
[95]S. Chavan, J. G. Vitillo, E. Groppo, F. Bonino, C. Lamberti, P. D. C. Dietzel and S. Bordiga *J. Phys. Chem. C* **113**, 3292 (2009).
[96]S. Chavan, F. Bonino, J. G. Vitillo, E. Groppo, C. Lamberti, P. D. C. Dietzel, A. Zecchina and S. Bordiga *Phys. Chem. Chem. Phys.* **11**, 9811 (2009).
[97]N. Masciocchi, S. Galli, V. Colombo, A. Maspero, G. Palmisano, B. Seyyedi, C. Lamberti and S. Bordiga *J. Am. Chem. Soc.* **132**, 7902 (2010).
[98]L. Mino, V. Colombo, J. G. Vitillo, C. Lamberti, S. Bordiga, E. Gallo, P. Glatzel, A. Maspero and S. Galli *Dalton Trans.* **41**, 4012 (2012).
[99]A. Rossin, B. Di Credico, G. Giambastiani, M. Peruzzini, G. Pescitelli, G. Reginato, E. Borfecchia, D. Gianolio, C. Lamberti and S. Bordiga *J. Mater. Chem.* **22**, 10335 (2012).
[100]T. D. Bennett, A. L. Goodwin, M. T. Dove, D. A. Keen, M. G. Tucker, E. R. Barney, A. K. Soper, E. G. Bithell, J. C. Tan and A. K. Cheetham *Phys. Rev. Lett.* **104**, 115503 (2010).